Lithuanian Journal of Physics, Vol. **61**, No. 4, pp. 251–260 (2021)

SYNTHESIS AND CHARACTERIZATION OF IRIDIUM-DOPED MULTI-WALLED CARBON NANOTUBES

E. Jakubovskij [a], A. Selskis [b], I. Ignatjev [c], G. Stalnionis [b], and V. Šablinskas [a]

[a] *Institute of Chemical Physics, Faculty of Physics, Vilnius University, Saulėtekio 3, 10257 Vilnius, Lithuania*

[b] *Department of Structural Analysis of Materials, Center for Physical Sciences and Technology, Saulėtekio 3, 10257 Vilnius, Lithuania*

[c] *Department of Organic Chemistry, Center for Physical Sciences and Technology, Saulėtekio 3, 10257 Vilnius, Lithuania*

Email: mail@eldar.jakubovskij.name

Received 4 August 2021; accepted 6 September 2021

Multi-walled carbon nanotubes have been prepared by chemical vapour deposition pyrolysis of ethyl alcohol at 665°C. The addition of atoms other than carbon to the nanostructure, in our case the iridium component, leads to the formation of defects that contribute to changes in the electrical and optoelectrical properties. The formation and structural changes of multi-walled nanotubes were studied using an electron microscope, Raman and energy-disperse spectrometry. Using the Raman and X-ray spectrum, a clear difference between the synthesis without and with the addition of iridium impurities was found.

Keywords: multi-walled carbon nanotubes (MWCNT), iridium-doped, nanohybrid composite, Raman spectrum, energy-dispersive X-ray spectroscopy

1. Introduction

Every carbon nanostructure brought new developments in research. One of impetus for the following decades was the study of the Japanese researcher Iijima on the formation of carbon structures in 1991, which were formed on the cathode when graphite was sprayed in an electric arc [1]. In turn, almost two centuries before the carbon nanostructures, iridium was discovered in 1803 by the English chemist S. Tennant along with osmium, which was present as impurities in natural platinum originating from South America. The first to admit that a small insoluble residue survived a dissolution of native platinum in aqua regia was the French chemist Joseph Louis Proust. In 1799, he described his black residue as 'nothing more than graphite or plumbago'. Tennant was the first among several scientists who managed to obtain an insoluble residue in sufficient quantities after dissolving platinum in aqua regia and to identify previously unknown metals in it [2].

Carbon nanostructures, including carbon nanotubes, are currently one of the active research areas. In 1889, Edison published the results of experiments on the thermal decomposition of methane in a light bulb, where carbon filaments were formed. In subsequent years, the study of the formation of carbon structures gradually grew. The literature on the study of the properties and applications of multilayer CNTs has advanced again in recent years, and recently there has been interest in improving and controlling their properties using various functionalization and doping methods. Modification of the structure of nanotubes by the controlled placement of defects, chemical groups or extraneous atoms entails technological consequences, in turn justifying a large number of experimental and

theoretical studies focused on these topics. A lot of work has already been done in the areas of intercalation, endohedral doping and replacement doping. Semiconductor electronics requires the use of both p-type and n-type semiconductors. These structural changes can be controlled by doping with electron-acceptor and electron-donor additives. The p-type doping can be carried out quite simply, since CNT naturally adsorbs molecular oxygen from the air. The alloying of the n-type CNT turned out to be more difficult in terms of the stability of doping and the general characteristics of the devices. Boron and nitrogen doping is used to create electrocatalysts for oxygen reduction reactions, hydrogen evolution, biological reactions and gas sensing [3–8]. B-doped CNTs show the best sensitivity to ethylene, while N-doped CNTs show the best sensitivity to nitrogen dioxide and carbon monoxide [9–13]. These modifications open up prospects for the use of CNTs in transistors, sensors, solar cells, optoelectronic and thermoelectric devices, charge-storage and fuel-storage devices [14–17]. Such an extensive range of semiconductor properties inspires scientists to develop hybrid and fully organic electronic devices [18–24]. The aim of this work was to study the formation of multi-walled carbon nanotubes by incorporating iridium atoms into the structure.

2. Synthesis. Materials and methods

Carbon nanotubes were synthesized using chemical pyrolysis on an iron substrate at atmospheric pressure using argon [25–31]. 95% ethanol was used as a carbon source. The mixture was fed in a reactor with a diameter of 25 mm. Before the process of chemical vapour deposition, the reactor system was cleaned with argon for 1 h with a flow of 53 ml/min. Ar/Ethanol vapour was introduced into a quartz tube with a flow of 47 ml/min. Two solutions of ethanol and iridium(IV) chloride were used. For chemical vapour deposition *Alfa Aesar* iridium(IV) chloride, 99.95% (metal basis), Ir 56.5% min was used. Before the pyrolysis process, a mixture of argon and ethanol was fed to the system for 7 min, after which it was placed in a cylindrical furnace with 665°C temperature. During the entire cooling period, the argon flow was not turned off to reduce the residues of chemical pyrolysis. The formed carbon nanotubes were studied using a Raman spectrometer *Renishaw* inVia Raman microscope, a scanning electron microscope *Helios* NanoLab 650, and an energy dispersive X-ray spectrometer INCAx-sight with a scanning electron microscope EVO-50.

3. Results and discussion

Carbon nanotubes grown on an iron substrate under the described conditions were initially studied using an electron microscope. The preliminary work for a careful selection of the pyrolysis process – growth temperature, flow rate and carbon carrier concentration in the flow – allowed establishing optimal conditions for the growth of iridium-doped carbon nanotubes. MWCNT was synthesized on stainless steel substrate from ethanol at 665°C temperature (Fig. 1). Figure 2 shows the Raman spectrum of a multi-walled carbon nanotube. After the synthesis, multi-walled carbon nanotubes were purified by a three-step process. Firstly, the obtained powder was heated in dry air for an hour at 400°C to remove amorphous carbon and graphitic carbon surrounding the iron particles. Secondly, nanotubes were immersed in HNO_3 and heated for 5 h at 85°C temperature to dissolve and remove iron and iron oxide particles. Finally, the remaining powder was washed with distilled water until it reached neutral pH. The samples were measured by a Raman spectrometer *Renishaw* under ambient conditions with a laser excitation of

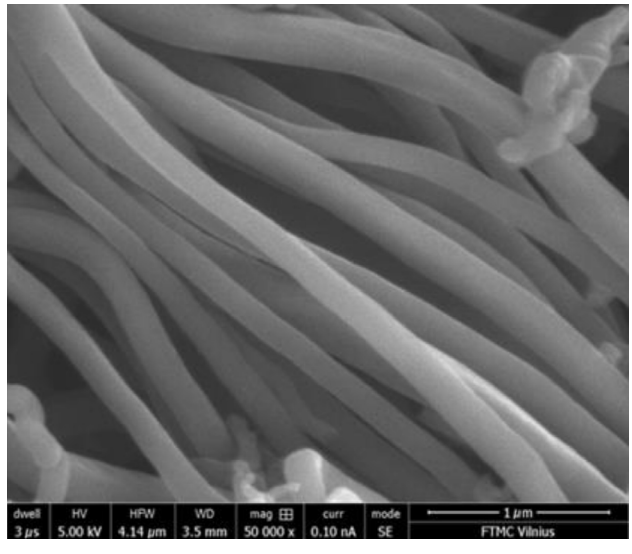

Fig. 1. SEM image of MWCNT synthesized from ethanol.

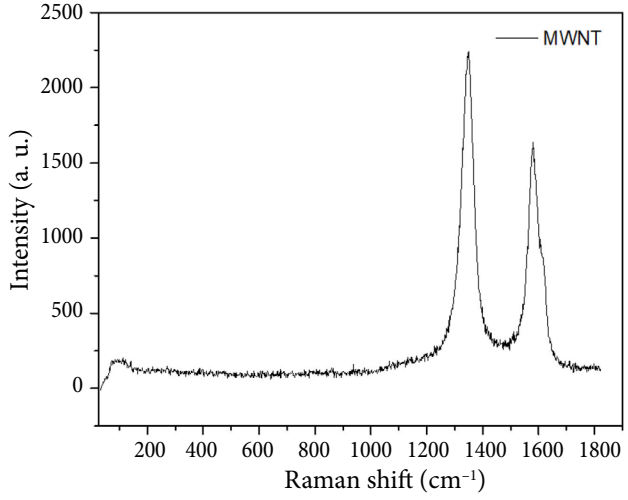

Fig. 2. Raman spectrum of MWCNT synthesized from ethanol.

532 nm, the calibration with Si showed 520 and 442 cm^{-1}, and the standard resolution mode was used for the measurement with the help of a ×50 objective (Figs 2, 3). The growing of carbon nanotubes with incorporated iridium consisted of several stages. Given many possible options for the formation of carbon nanotubes on an iron substrate, the result of long and short synthesis processes differs from each other not only by the difference between the length of the nanotubes themselves, but also by the structure. Separate results, further described in the work, as it happened earlier, raised new questions and revealed some more information about the structure of multi-walled carbon nanotubes. Structurally changing the carbon tubular shape of the nanotubes by adding the so-called 'defects', we obtain new structures that are formed with different from the previous physical properties. Most of these defects can be ascertained using Raman spectrometry [32–35]. Further, these results tell about one of these structural changes. Figure 4 shows the initial phase of the formation of multi-walled nanotubes with adding an iridium component to the synthesis process. In the Figure, there are visible twisted, climbing, tilting multi-walled carbon nanotubes with a diameter of 100–150 nm. As can be seen from the electron microscope image, the initial stage of the formation of MWCNT indicates structural 'defects' that will be repeated during a longer process, thereby establishing the stability of the process. We see the formed short multi-walled carbon nanotubes after 5 min of the synthesis from ethanol and iridium chloride mixtures. The difference in the diameter of CNT depends on the surface structure of the iron substrate, also on the flow rate of the mixture, and it is very dependent on temperature. Increasing the temperature, the diameter of nanotubes decreases. The following Figs. 5 and 6 show the spectral measurements of various layers of multi-walled carbon nanotubes after the chemical vapour deposition for 15 and 50 min (Fig. 7), and 5 h. The pyrolysis process temperature was 665°C and the flow rate of argon and ethanol–iridium mixture was 53 ml/min. Raman spectral analysis was performed using laser radiation at 532 nm in ambient conditions. The presented comparison of the Raman spectrum of iridium-incorporating carbon nanotubes after different synthesis times shows a change

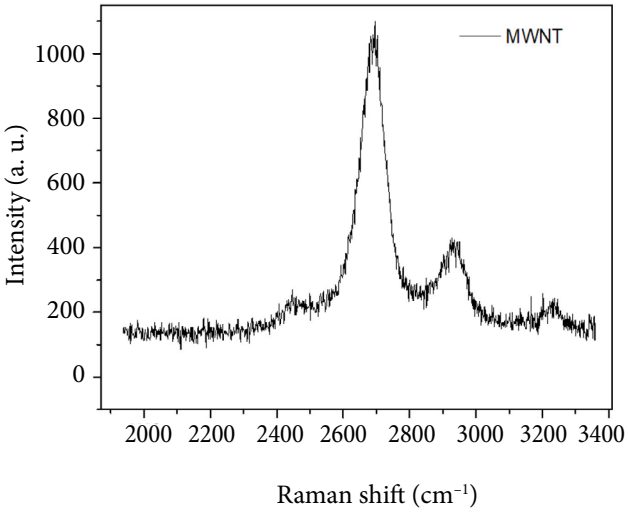

Fig. 3. Raman spectrum of MWCNT synthesized from ethanol.

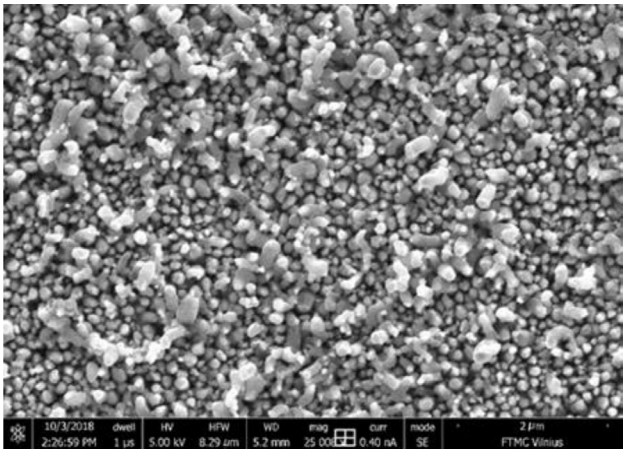

Fig. 4. SEM image of MWCNT after 5 min growing (gas flow 47 ml/min).

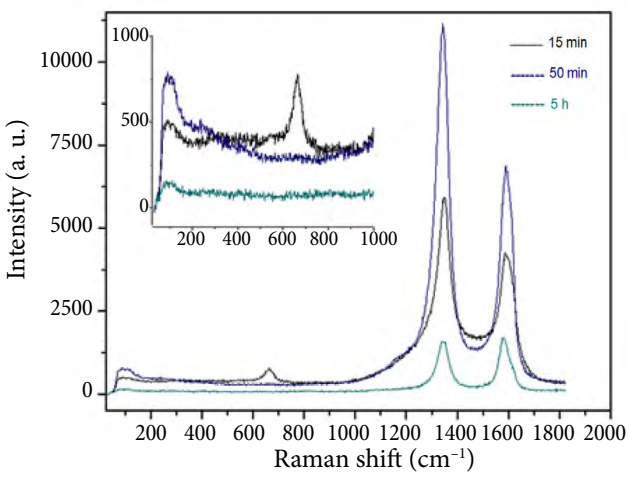

Fig. 5. Raman spectra of MWCNT after 15 min, 50 min and 5 h growing.

in the RBM, D, G, G', D', G+D, 2D and 2G modes. It can be seen from the graph that the value of the RBM mode in the second sample differs from those of the first and third samples. D, G and D' modes are clearly distinguishable in all three spectra: 15 min growing – 101, 664, 1348, 1590, 1615 cm^{-1}; 50 min – 101, 1342, 1590, 1615 cm^{-1}; 5 h – 101, 1342, 1580, 1612 cm^{-1}. In the first sample, one more line is clearly visible, which appeared after the iridium compound was added to the process of chemical pyrolysis. The spectra show two intensive peaks at 1348 and 1590 cm^{-1}, corresponding to the disorder-induced sp^2 peak (D-line) and the graphite highly oriented mode sp^2 peak (G-line). The relationship between the D and G lines

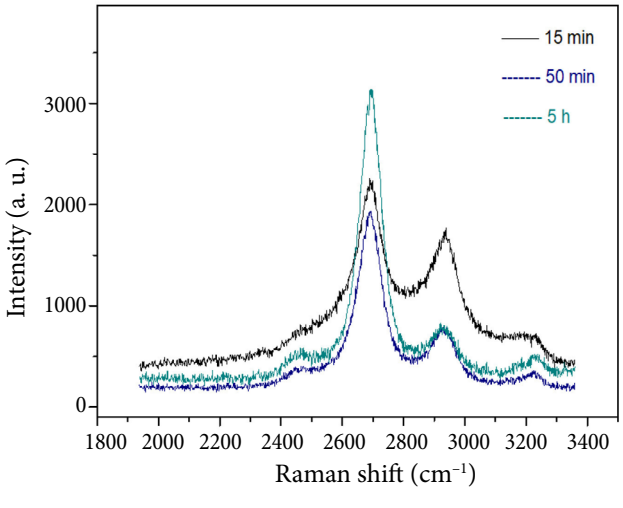

Fig. 6. Raman spectra of MWCNT after 15 min, 50 min and 5 h growing.

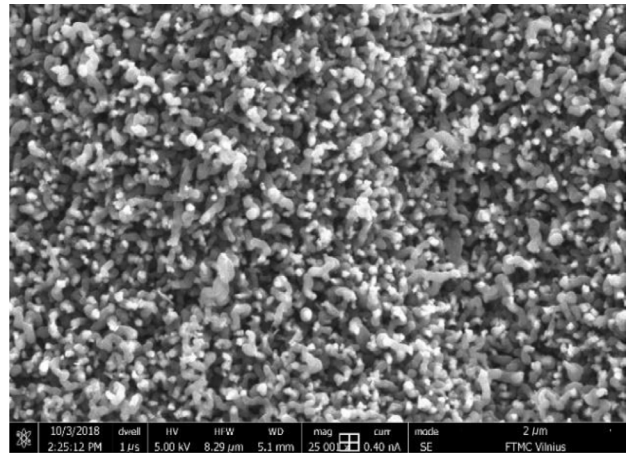

Fig. 7. SEM image of MWCNT after 50 min synthesis.

gives information about the structure of the sample data. The intensity of the D peak is greater compared to that of the G peak, which indicates a certain level of the C–C sp^2 order. A high level of crystallinity of the tubes is described by a decrease in the D peak. The presence of the shoulder D' in a 5-hour sample indicates a low degree of the order of C–C sp^2. In the far part of the spectrum, the 2D, G+D and 2G modes are clearly pronounced: 15 min growing – 2694, 2932, 3230 cm^{-1}; 50 min – 2689, 2925, 3227 cm^{-1}; 5 h – 2690, 2937, 3225 cm^{-1}. The peak, which is newly formed in the process, is related to the structural change of the tubular form of carbon nanotubes. The peak at 664 cm^{-1} indicates a different bond between the atoms involved in the synthesis process. The specific ability of carbon and iridium atoms to attach, as well as the low crystallinity of the nanostructures obtained, may indicate the formation of more carbon-free regions in the nanotubes, with iridium replacing carbon. Given a small change in the RBM mode, the MWCNT structure formed consists of carbon and iridium atoms. One of the formations may be a structure with incomplete bonds of iridium, that is, carbon. The image of the electron microscope in Fig. 4 shows that the synthesized nanotubes consist of the configuration of a single layer of graphite, as well as of the defective areas, which lead to the twisting of the tubular shape. In the process of pyrolysis, the structure of MWCNT changes the offset of addition of extra doping atoms, also because of the tendency of the crystal lattice towards a more stable state. The above peak may refer to the formation of a lattice such that the double-bond iridium atom is connected to the 'benzene' rings of carbon.

The remaining two bonds can also consist of a bond with carbon with either chlorine or oxygen. At 665°C temperature, ethanol and iridium chloride are disintegrated into components, after which free hydrogen, chlorine and oxygen form hydrochloric acid and water, and also radicals. Quantifying the finding of atoms other than carbon is quite a challenge when resorting to measuring only the Raman spectrum. One of the methods for the quantitative determination of atoms is the method of energy-dispersive X-ray spectroscopy. The EDS spectrum of the sample after 5 h of growth is presented in Fig. 8. The spectra indicate the dominant carbon component and the presence of iron, oxygen and iridium. Taking into account the possibilities of this method in analyzing samples or, more precisely, in determining the presence of atoms on the surface, it can be determined that after a long 5-hour synthesis process iron appears, which participates in the formation of nanotubes, and also iridium and oxygen. The oxygen component can be easily explained given the fact that carbon nanotubes, after molding, cooling, annealing and cleaning, are capable of attaching oxygen under ambient conditions. In turn, the iridium component is several orders of magnitude smaller than the oxygen one. This value of 0.03 percent mass fraction of the total measured carbon mass indicates the presence of iridium in the final phase in the formation of carbon nanotubes. The following Figs. 9, 10 and 11 show information about the synthesis process, in which the iridium component is even more visible. Figures 9 and 10 show the Raman spectrum of other samples synthesized with a different mixture. RBM, D, G and D′ modes of multi-walled carbon nanotubes are the following: 15 min growing – 101, 305, 428, 658, 1345, 1599, 1615 cm^{-1}; 50 min – 101, 664, 1345, 1580, 1612 cm^{-1}; 5 h – 101, 1345, 1580, 1615 cm^{-1}. Comparing the spectral measurements of the two synthesis methods, one can immediately notice the difference between the spectra of 50-minute synthesis. A peak appears at 658 cm^{-1}, which is close to a peak of 664 cm^{-1}. The subtle peaks at 306 and 428 cm^{-1} relate to iron oxide, which is formed as a by-product during the pyrolysis process. In addition, as can be seen in Fig. 9, the peak at 306 cm^{-1} can be attributed to $IrCl_4$, which is in the pyrolysis mixture. In the reactor

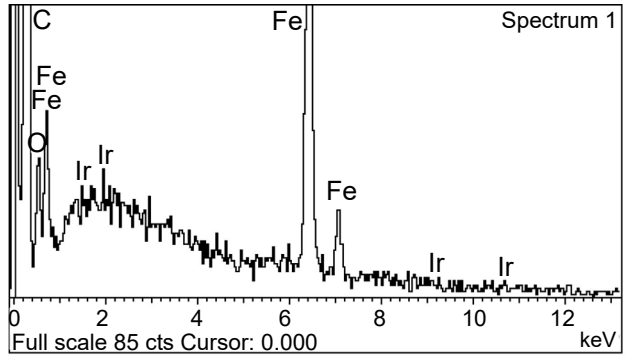

Element	Weight%	Atomic%
C K	89.50	95.72
O K	3.26	2.62
Fe K	7.21	1.66
Ir M	0.03	0.00
Totals	100.00	

Fig. 8. EDS spectrum of MWCNT after 5 h synthesis.

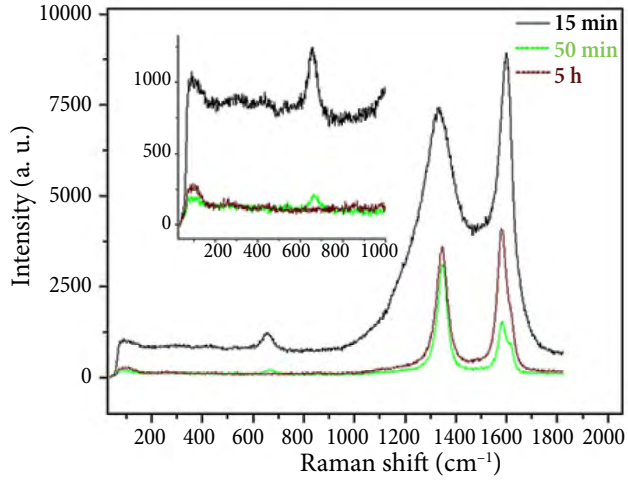

Fig. 9. Raman spectrum of Ir-doped MWCNT.

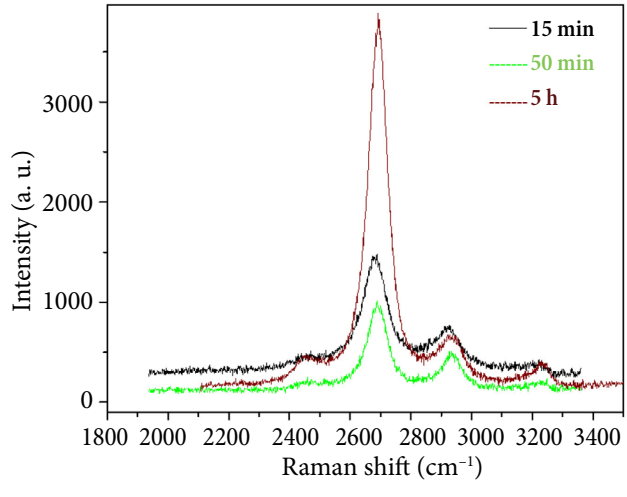

Fig. 10. Raman spectrum of Ir-doped MWCNT.

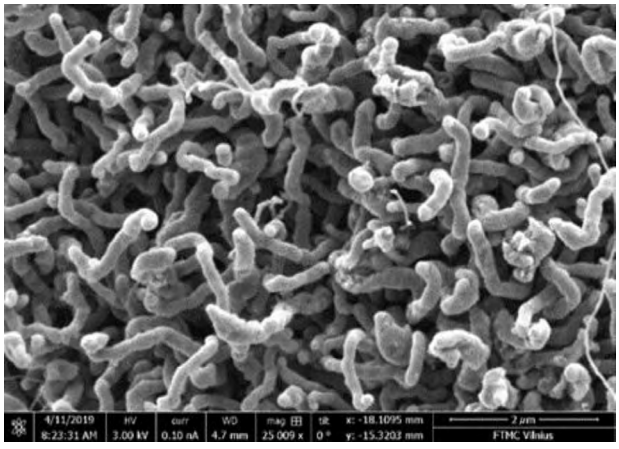

Fig. 11. SEM image of MWCNT after 5 h synthesis.

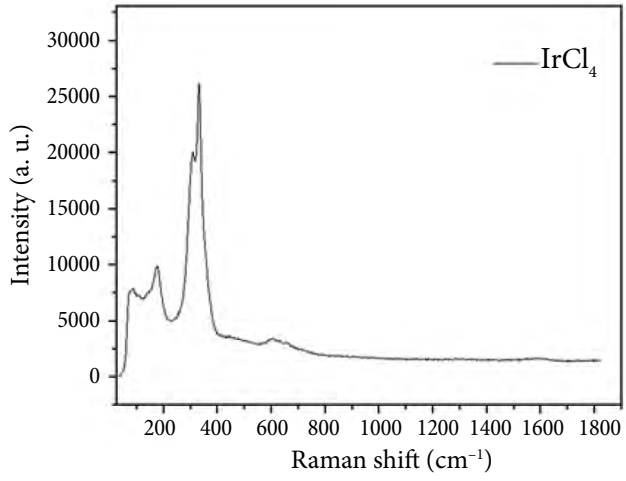

Fig. 12. Raman spectra of $IrCl_4$ in standard conditions, laser excitation 532 nm.

after the disintegration of ethanol, free oxygen atoms are formed. During the pyrolysis process, oxygen interacts with hydrogen, carbon, iron and iridium. After evaluating the X-ray spectrum, it becomes clear that iridium and iron oxides are also present in the formed layers of carbon nanotubes. There are also several iridium compounds: Ir–O, Ir–Cl, Ir–C. With a high probability, all these compounds are present in the carbon layer. They were even less distinguishable in the spectrum indicated in Fig. 9. As we can see, the manifestation of a peak at 664 cm^{-1} occurs in the second case, although such a peak is not observed in the 5-hour process. Certainly, the fact that one of the peaks of iron oxide (Fe_2O_3) is also located in this zone complicates the task of determination [34]. There is also a very small difference in the RBM mode, which varies between 101±7 cm^{-1}. The values of D, G and D' modes are identical at 1345, 1596 and 1612 cm^{-1}, respectively. Compared with the first measurements, a peak at 664 cm^{-1} appeared after 15 and 50 min of synthesis. Measurements of the MWCNT spectrum after a longer synthesis process did not reveal this peak. Figure 11 shows an image of the electron microscope of the initial stage of nanotube synthesis at the second ratio of iridium chloride and ethyl alcohol. The measurement and analysis of the Raman spectrum used in the synthesis of iridium chloride partially confirms the abovementioned results. Figures 12 and 13 present the Raman spectrum of iridium chloride. Taking into account the hygroscopicity of iridium chloride and the standard conditions in which the measurements were made, the Raman spectrum is as accurate as possible, since the substance was isolated from air before the measurements. The value of an indistinguishable peak at 607 cm^{-1} may indicate that iridium chloride is present during the formation of carbon nanotubes and is deposited on the surface. However, the difference between these two peaks at 607 and 664 cm^{-1} indicates a different connection. In Figures 5 and 9, during the synthesis at 15 and 50 min, the same line is clearly visible at 664±7 cm^{-1}, describing a different atomic bond. According to Huang et al., materials such as iridium oxide have four active Raman modes. For iridium oxide, they appear at 145, 561, 752 and 728 cm^{-1}. In addition, the peaks appearing at 366 and 456 cm^{-1} are usually described by the stretching mode Ir = O in the amorphous phase and

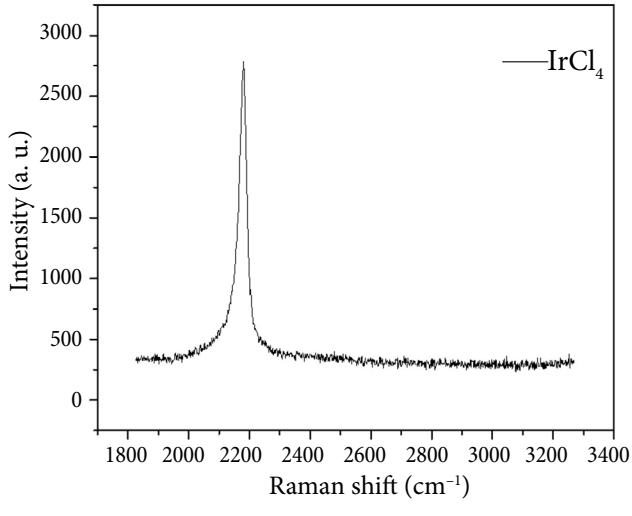

Fig. 13. Raman spectra of $IrCl_4$ in standard conditions, laser excitation 532 nm.

the stretching mode Ir–O, respectively [36, 37]. The measured spectrum of $IrCl_4$ shows peaks at 81, 177, 306, 333, 607 and 2177 cm^{-1}. The most important are the peaks at 81 and 607 cm^{-1} since one of them, namely, the peak at 81 cm^{-1}, intersects with the peak of carbon nanotubes at 101 cm^{-1}. Such a slight difference in the iridium peak and the RBM modes of carbon nanotubes on the Raman spectrum is almost impossible to distinguish. However, bearing in mind that the process of growing carbon nanotubes takes place at the temperature close to that at which iridium chloride is disintegrating into its constituent elements, it can be assumed that the change in the RBM mode of MWCNT results in the addition of iridium to the carbon structure. The D, G and D' modes of carbon nanostructures in the second synthesis variant are defined as 1345, 1596 and 1612 cm^{-1} within 7 units, compared to the MWCNT modes related to the samples of the first synthesis – 1351, 1590 and 1615 cm^{-1}. Figure 14 shows the X-ray spectrum of the second sample after 5 h of the synthesis. During the chemical pyrolysis of the second samples, a solution of ethanol was used with an increased amount of iridium chloride, which is traced in the figure. The iridium component is very small compared to the dominant carbon, also with iron and oxygen. However, the previous results suggest that a carbon–iridium compound may occur in the structure of MWCNT.

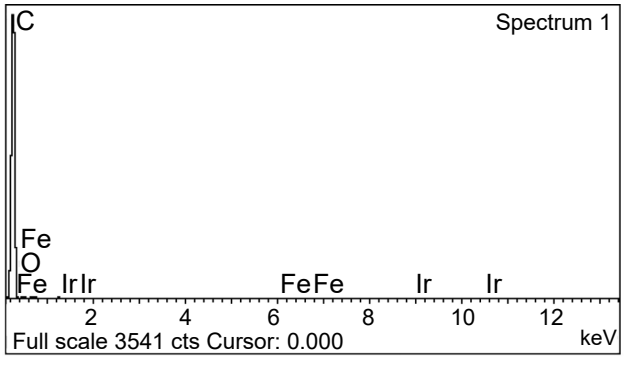

Element	Weight%	Atomic%
C K	94.66	97.75
O K	1.95	1.51
Fe L	3.30	0.73
Ir M	0.09	0.01
Totals	100.00	

Fig. 14. EDS spectra of MWCNT after 5 h synthesis.

4. Conclusions

This paper presents the studies of structural changes in the multi-walled carbon nanotubes synthesized from ethanol using chemical vapour deposition. We investigated the formation of carbon nanotubes under certain conditions, adding iridium chloride to the carbon source, and established the differences of the formation between the processes of short and long syntheses from the resulting mixture. Using the Raman and X-ray spectrum, a clear difference was found between the synthesis without and with adding iridium impurities. In turn, the Raman measurements of grown nanotubes revealed the changes in the spectra, that allowed us to answer some questions related to the formation of nanostructures. The revealed peaks at 664 and 658 cm^{-1} suggest a new formation that has not previously been observed. The formation of n-type carbon nanotubes makes it possible to enhance the donor properties, that lead to changes in their electrical and optoelectrical properties, which can be applied in organic structures starting from transistors, solar cells and detectors, as well as in biological nano-systems of a molecular level and superconductors. The synthesis of carbon nanotubes and doping remains a studied field of science. Undoubtedly, the results obtained using the energy-dispersive X-ray spectrometry method provide only a partial determination of the existence of multi-walled carbon nanotubes doped with iridium. The use of energy-dispersed spectrum analysis is one of the methods for determining the presence of carbon and iridium compounds in the MWNT obtained by the process of chemical vapour deposition.

References

[1] S. Iijima, Helical microtubules of graphitic carbon, Nature **354**, 6348 (1991), https://doi.org/10.1038/354056a0

[2] S. Tennant, On two metals, found in the black powder remaining after the solution of platina, Philos. Trans. R. Soc. Lond. **94**, 1776–1886 (1804), https://doi.org/10.1098/rstl.1804.0018

[3] P.G. Collins, K. Bradley, M. Ishigami, and A. Zettl, Extreme oxygen sensitivity of electronic properties of carbon nanotubes, Science

287, 5459 (2000), https://doi.org/10.1126/science.287.5459.1801

[4] S. Ratso, I. Krussenberg, M. Vikkisk, U. Joost, E. Shulga, I. Kink, T. Kallio, and K. Tammeveski, Highly active nitrogen-doped few-layer graphene/carbon nanotube composite electrocatalyst for oxygen reduction reaction in alkaline media, Carbon **73**, 361–370 (2014), https://doi.org/10.1016/j.carbon.2014.02.076

[5] K. Yokoyama, S. Yokoyama, Y. Sato, K. Hirano, S. Hashiguchi, K. Motomiya, H. Ohta, H. Takahashi, K. Tohji, and Y. Sato, Efficiency and long-term durability of a nitrogen-doped single-walled carbon nanotube electrocatalyst synthesized by defluronation-assisted nanotube-substitution for oxygen reduction reaction, J. Phys. Chem. A **4**, 9184–9195 (2016), https://doi.org/10.1039/C6TA02722A

[6] D.J. Li, U.N. Maiti, J. Lim, D.S. Choi, W.J. Lee, Y. Oh, G.Y. Lee, and S.O. Kim, Molybdenum sulfide/N-doped CNT forest hybrid catalysts for high-performance hydrogen evolution reaction, Nano Lett. **14**, 1228–1233 (2014), https://doi.org/10.1021/nl404108a

[7] J.-J. Adjizian, R. Leghrib, A.A. Koos, I. Suarez-Martinez, A. Crossley, Ph. Wagner, N. Grobert, E. Lobet, and Ch.P. Ewels, Boron and nitrogen-doped multiwalled carbon nanotubes for gas detection, Carbon **66**, 662–673 (2014), https://doi.org/10.1016/j.carbon.2013.09.064

[8] F.G. Pachecoa, A.A.C. Cottaa, H.F. Gorgulhob, A.P. Santosa, W.A.A. Macedoa, and C.A. Furtado, Comparative temporal analysis of multiwalled carbon nanotube oxidation reactions: Evaluating chemical modifications on true nanotube surface, Appl. Surf. Sci. **357**, 1015–1023 (2015), https://doi.org/10.1016/j.apsusc.2015.09.054

[9] L. Brownlie and J. Shapter, Advances in carbon nanotube n-type doping: Methods, analysis and applications, Carbon **126**, 257–270 (2018), https://doi.org/10.1016/j.carbon.2017.09.107

[10] B. Bauerhenne, E.S. Zijlstra, A. Kalitsov, and M.E. Garcia, Controlling three laser-excited coherent phonon modes in boron nitride nanotubes to produce ultrashort shaped terahertz pulses: implications for memory devices, ACS Appl. Nano Mater. **1**(12), 6932–6937 (2018), https://doi.org/10.1021/acsanm.8b01716

[11] Y. Nonoguchi, K. Ohashi, R. Kanazawa, K. Ashiba, K. Hata, T. Nakagawa, Ch. Adachi, T. Tanase, and T. Kawai, Systematic conversion of single walled carbon nanotubes into n-type thermoelectric materials by molecular dopants, Sci. Rep. **3**, 3344 (2013), https://doi.org/10.1038/srep03344

[12] R. Czerw, M. Terrones, J.C. Charlier, X. Blase, B. Foley, R. Kamalakaran, N. Grobert, H. Terrones, D. Teklea, P.M. Ajayan, W. Blau, M. Rühle, and D.L. Carroll, Identification of electron donor states in n-doped carbon nanotubes, Nano Lett. **1**(9), 457–460 (2001), https://doi.org/10.1021/nl015549q

[13] H. Cui, X. Zhang, J. Zhang, and M.A. Mehmood, Interaction of CO and CH_4 adsorption with noble metal (Rh, Pd, and Pt)-decorated N_3-CNTs: A first-principles study, ACS Omega **3**(12), 16892–16898 (2018), https://doi.org/10.1021/acsomega.8b02578

[14] X. Zhang, X. Yin, J. Luo, X. Zheng, H. Wang, J. Wang, Z. Xi, X. Liao, J. Ong'achwa Machuki, K. Guo, and F. Gao, Novel hierarchical nitrogen-doped multiwalled carbon nanotubes/cellulose/nanohydroxyapatite nanocomposite as an osteoinductive scaffold for enhancing bone regeneration, ACS Biomater. Sci. Eng. **5**(1), 294–3071 (2019), https://doi.org/10.1021/acsbiomaterials.8b00908

[15] D. Maiti, X. Tong, X. Mou, and K. Yang, Carbon-based nanomaterials for biomedical applications: A recent study, Front. Pharmacol. **9**, 1401 (2019), https://doi.org/10.3389/fphar.2018.01401

[16] D.C. Higgins, D. Meza, and Z. Chen, Nitrogen-doped carbon nanotubes as platinum catalyst supports for oxygen reduction reaction in proton exchange membrane fuel cells, J. Phys. Chem. C **114**, 21982–21988 (2010), https://doi.org/10.1021/jp106814j

[17] C.K. Acharya and C.H. Turner, Effect of an electric field on the adsorption of metal clusters on boron-doped carbon surfaces, J. Phys. Chem. **111**, 14804–14812 (2007), https://doi.org/10.1021/jp073643a

[18] W. Zhang, X. Zhang, L. Chen, J. Dai, Y. Ding, L. Ji, J. Zhao, M. Yan, F. Yang, Ch.-R. Chang, and S. Guo, Single-walled carbon nanotube induced optimized electron polarization of rhodium nanocrystals to develop an interface catalyst for highly efficient electrocatalysis, ACS Catal. **8**(9), 8092–80999 (2018), https://doi.org/10.1021/acscatal.8b02016

[19] Z. Wang, S. Peng, Y. Hu, L. Li, T. Yan, G. Yang, D. Ji, S. Madhavi, Z. Pan, and S. Ramakrishna, Cobalt nanoparticles encapsulated in carbon nanotube-grafted nitrogen and sulfur co-doped multichannel carbon fibers as efficient bifunctional oxygen electrocatalysts, J. Mat. Chem. **5**(10), 4949–4961 (2017), https://doi.org/10.1039/C6TA10291C

[20] R. Arrigo, M.E. Schuster, Z. Xie, Y. Yi, G. Wowsnick, L.L. Sun, K.E. Hermann, M. Friedrich, P. Kast, M. Hävecker, A. Knop-Gericke, and R. Schlögl, Nature of the N–Pd interaction in nitrogen-doped carbon nanotube catalysts, ACS Catal. **5**(5), 2740–2753 (2015), https://doi.org/10.1021/acscatal.5b00094

[21] H. Li, P. Tao, Y. Xu, X. Zhang, S. Liu, and Q. Zhao, Solution-processable high-efficiency bis(trifluoromethyl)phenyl functionalized phosphorescent neutral iridium (III) complex for greenish yellow electroluminescence, Tetrahedron Lett. **59**, 1748–1751 (2018), https://doi.org/10.1016/j.tetlet.2018.03.073

[22] W. Lei, W. Xiao, J. Li, G. Li, Z. Wu, C. Xuan, D. Luo, Y.-P. Deng, D. Wang, and Z. Chen, Highly nitrogen-doped three-dimensional carbon fibers network with superior sodium storage capacity, ACS Appl. Mater. Interfaces **9**(34), 28604–28611 (2017), https://doi.org/10.1021/acsami.7b08704

[23] W.-K. Hua, S.-H. Li, X.-F. Ma, S.-X. Zhou, Q.-F. Zhang, J.-Y. Xu, P. Shi, B.-H. Tong, M.-K. Fung, and L. Fu, Blue-to-green electrophosphorescence from iridium (III) complexes with cyclometalated pyrimidine ligands, Dyes Pigm. **150**, 284–292 (2018), https://doi.org/10.1016/j.dyepig.2017.12.020

[24] L. Gao, P. Tao, Y. Miao, W. Jia, Y. Zhao, H. Wanga, and B. Xu, Sky-blue phosphorescent organic light-emitting diode with superior performance based on novel chlorine functionalized iridium (III) complex, Tetrahedron Lett. **59**, 2095–2098 (2018), https://doi.org/10.1016/j.tetlet.2018.04.053

[25] Q. Zhao, Z. Xu, Y. Hu, F. Ding, and J. Zhang, Chemical vapor deposition synthesis of near-zigzag single-walled carbon nanotubes with stable tube-catalyst interface, Sci. Adv. **2**, e1501729–e1501729 (2016), https://doi.org/10.1126/sciadv.1501729

[26] J. Robertson, G. Zhong, S. Esconjauregui, C. Zhang, M. Fouquet, and S. Hofmann, Chemical vapor deposition of carbon nanotube forests, Phys. Status Solidi B **249**(12), 2315–2322 (2012), https://doi.org/10.1002/pssb.201200134

[27] B. Chen, C. Zhang, S. Esconjauregui, R. Xie, G. Zhong, S. Bhardwaj, C. Cepek, and J. Robertson, Carbon nanotube forests growth using catalysts from atomic layer deposition, J. Appl. Phys. **115**, 144303 (2014), https://doi.org/10.1063/1.4870951

[28] S. Dörfler, A. Meier, S. Thieme, P. Németh, H. Althues, and S. Kaskel, Wet-chemical catalyst deposition for scalable synthesis of vertical aligned carbon nanotubes on metal substrates, Chem. Phys. Let. **511**, 288–293 (2011), https://doi.org/10.1016/j.cplett.2011.06.027

[29] C. Liu and H.M. Cheng, Carbon nanotubes: controlled growth and application, Mat. Today **16**, 19–28 (2013), https://doi.org/10.1016/j.mattod.2013.01.019

[30] M. Zhang and J. Li, Carbon nanotube in different shapes, Mat. Today **12**(6), 12–18 (2009), https://doi.org/10.1016/S1369-7021(09)70176-2

[31] E.-X. Ding, Q. Zhang, N. Wei, A.T. Khan, and E.I. Kauppinen, High-performance single-walled carbon nanotube transparent conducting film fabricated by using low feeding rate of ethanol solution, R. Soc. Open Sci. **5**, 180392 (2018), https://doi.org/10.1016/j.jmst.2019.07.011

[32] Z. Zhao, Z. Yang, Y. Hu, J. Li, and X. Fan, Multiple functionalization of multi-walled carbon nanotubes with carboxyl and amino groups, Appl. Phys. Sci. **276**, 476–481 (2013), https://doi.org/10.1016/j.apsusc.2013.03.119

[33] A.J. Pool, S.K. Jain, and G.T. Barkema, Structural characterization of carbon nanotubes via the vibrational density of states, Carbon **118**, 58–65 (2017), https://doi.org/10.1016/j.carbon.2017.03.030

[34] N. Soin, S.S. Roy, S.C. Ray, and J.A. McLaughlin, Excitation energy dependence of Raman bands in multiwalled carbon nanotubes, J. Raman Spectrosc. **41**(10), 1227–1233 (2010), https://doi.org/10.1002/jrs.2594

[35] Z. Li, R. Little, E. Dervishi, V. Saini, Y. Xu, and A.R. Biris, Micro-Raman spectroscopy analysis of catalyst morphology for carbon nanotubes synthesis, Chem. Phys. **353**, 25–31 (2008), https://doi.org/10.1016/j.chemphys.2008.07.013

[36] S. Thanawala, D.G. Georgiev, R.J. Baird, and G. Auner, Characterization of iridium oxide thin films deposited by pulsed-direct-current reactive sputtering, Thin Solid Films **515**, 7059–7065 (2007), https://doi.org/10.1016/j.tsf.2007.02.090

[37] R.K. Kawar, P.S. Chigare, and P.S. Patil, Substrate temperature dependent structural, optical and electrical properties of spray deposited iridium oxide thin films, Appl. Surf. Sci. **206**, 90–101 (2003), https://doi.org/10.1016/S0169-4332(02)01191-1

DAUGIASIENIŲ ANGLIES NANOVAMZDELIŲ SU IRIDŽIO PRIEMAIŠOMIS SINTEZĖ IR CHARAKTERIZAVIMAS

E. Jakubovskij [a], A. Selskis [b], I. Ignatjev [c], G. Stalnionis [b], V. Šablinskas [a]

[a] *Vilniaus universiteto Fizikos fakulteto Cheminės fizikos institutas, Vilnius, Lietuva*

[b] *Fizinių ir technologijos mokslų centro Medžiagų struktūrinės analizės skyrius, Vilnius, Lietuva*

[c] *Fizinių ir technologijos mokslų centro Organinės chemijos skyrius, Vilnius, Lietuva*

Santrauka

Daugiasieniai anglies nanovamzdeliai buvo gauti etilo alkoholio cheminio garų nusodinimo (pirolizės) būdu 665 °C temperatūroje. Prie nanostruktūros pridedant kitų atomų, mūsų atveju – iridžio komponentą, susidaro defektai, kurie lemia elektrinių ir optoelektrinių savybių pokyčius. Daugiasienių nanovamzdelių susidarymas ir struktūriniai pokyčiai buvo tiriami naudojant elektroninį mikroskopą, Ramano ir energijos dispersijos spektrometrijas. Ramano ir rentgeno spindulių spektrai parodė iridžio priemaišos įnašą į sintezės procesą.